Journal of
MATERIALS RESEARCH

Control of cobalt nanoparticle size by the germ-growth method in inverse micelle system: Size-dependent magnetic properties

X. M. Lin and C. M. Sorensen
Condensed Matter Laboratory, Department of Physics, Kansas State University, Manhattan, Kansas 66506

K. J. Klabunde
Department of Chemistry, Kansas State University, Manhattan, Kansas 66506

G. C. Hajipanayis
Department of Physics and Astronomy, University of Delaware, Newark, Delaware 19716

(Received 1 May 1998; accepted 22 October 1998)

Control of Co particle size was archived by a germ-growth method during inverse micelle synthesis. Magnetic coercivity and blocking were both a function of the particle size, which ranged from 38 to 88 Å. Interparticle dipolar interaction was proven to be important in order to interpret the magnetic properties for large-size particles.

I. INTRODUCTION

Research during the last decade has demonstrated that nanosize semiconductor and metal particles have unique properties compared to the bulk materials, largely due to their small size and high surface to volume ratio.[1] Fundamentally, as we decrease the size, the electronic structure changes from continuous bands of the bulk material to discrete energy levels of atoms.[2] It is therefore no surprise to find that nanoparticles, which are a bridge between the bulk and the atomic state, have a significant size dependence for electrical, optical, magnetic, and chemical properties. Examples include the red shift of the photoluminescence peak in semiconductor nanoparticles is strongly dependent on the particle size,[3] magnetic nanoparticles prepared in gas phase have a size-dependent enhanced magnetic moment,[4] and dissociate chemisorption of D_2 was found to occur with great sensitivity to the size of iron, cobalt, and niobium nanoparticle catalyst.[5] Therefore, control of nanoparticle size is crucial in studying their properties.

The inverse micelle technique has been established as a simple method to obtain bulk quantities of nanoparticles.[6] The size of particles synthesized inside the inverse micelle can be varied by changing the [water]/[surfactant] ratio. An increase of the ratio increases the size of the water pool inside the inverse micelle, and therefore allows bigger particles to form. Pileni *et al.*[7] have used this method to synthesize different sizes of metal and semiconductor nanoparticles. We have synthesized cobalt nanoparticles in the inverse micelle system using $NaBH_4$ reduction of Co^{2+} ions and studied the morphology and magnetic properties of particles formed at different temperatures.[8] Unfortunately, the size of the cobalt particles prepared in this manner cannot be adjusted by changing the [water]/[surfactant] ratio, since it has been already proven that the final product of BH_4^- reduction is very sensitive to the [water]/[surfactant] ratio.[9] A high concentration of water would form Co_2B rather than Co metal inside the micelle. The purpose of this paper is to demonstrate that the average particle size in the inverse micelle can also be varied by a germ-growth method, within a certain size range, while keeping the [water]/[surfactant] ratio constant. As the name implies, particles can be germinated in the first stage of the reaction, and these seed particles are used as nucleation sites to grow larger size particles. We also study the magnetic properties of Co particles as a function of size. In Sec. II, we discuss the experimental procedures. In Sec. III, some experimental results are presented. Finally, in Sec. IV, the work is summarized and possible future work is discussed.

II. EXPERIMENTAL SECTION

The surfactant didodecyldimethylammonium bromide (DDAB) (98%) was purchased from Fluka and used as obtained. Solvent toluene was obtained from Fisher and further purified by distillation. $CoCl_2 \cdot 6H_2O$ (98%) and $NaBH_4$ (99%) were purchased from Aldrich and used as obtained. All the synthesis steps were carried out in an Ar environment to avoid possible oxygen contamination. 4.5 g DDAB was dissolved in toluene to obtain a 31.2 mL, 0.3 M micelle solution. 71.94 mg $CoCl_2 \cdot 6H_2O$ was then added to 30 mL of the clear micelle solution. The mixture was then sonicated until all the solid disappeared and a clear blue solution was obtained.

As we have shown in our previous work,[8] isolated single cobalt particles with fcc structure can be formed at temperatures lower than 20 °C. When the reaction temperature increases from 20° to approximately 35 °C, small clusters with a limited number of monomers start to appear. If the reaction temperature goes beyond 35 °C,

clusters dominate the final product. Within the temperature region where single particles are formed (below 20 °C), both the particle size and polydispersity slightly increase when we increase the reaction temperature. The success of the germ-growth procedure, as we observed during our experiments, largely depends on the size and uniformity of the seed particles synthesized in the first step. Therefore, all the syntheses were carried out below 15 °C to ensure small uniform particle formation after the first step of the reaction. During each of the following steps, the amount of $NaBH_4$ added was determined by the molar ratio $[Co^{2+}]:[BH_4^-] = 1:3$ to ensure a complete reduction of cobalt ions. **Step 1**: 300 μL of the 1 M $NaBH_4$ aqueous solution was slowly added to 10 mL $CoCl_2 \cdot 6H_2O$ micelle solution using a Hamilton microsyringe while vigorously stirring the solution with a magnetic stirring bar. The solution changed into a black colloid after one to two minutes. The colloid was stirred for another 15 min to ensure a complete reaction. **Step 2**: 5 mL of the black colloid was taken out from the reaction mixture and dried in an Ar environment. Another 5 mL $CoCl_2 \cdot 6H_2O$ micelle solution was slowly added to the remaining 5 mL of colloid while stirring. Then 150 μL of the 1 M $NaBH_4$ aqueous solution was added to the reaction mixture. The colloid was stirred for another 15 min. The same procedure in step 2 was repeated two more times. After each reaction step, one drop of colloid was diluted for later transmission electron microscopy (TEM) examination. All the TEM examinations were done with a Philips 201 electron microscope. Magnetic data were obtained using dried powder samples with a Quantum Design MPMS SQUID magnetometer.

III. RESULTS

A. Particle size variation

TEM images of particles synthesized in each reaction step under a reaction temperature of 10 °C are shown in Fig. 1. After the first step of the reaction, particles with an average diameter of 38 Å and a narrow distribution were formed. These particles were used as nuclei to grow larger particles. During the following steps, the average particle diameter increased from 38 to 76 Å. Experiments also showed that the size of the seed particles prepared in the first step is sensitive to the reaction temperature. A small increase of the reaction temperature can increase the particle size. Another group of samples synthesized at 12 °C showed average particle size varies from 44 to 88 Å.

The diameter of the colloidal particles can be calculated from conservation of mass as[10]

$$d_2 = d_1 \sqrt[3]{\frac{n_i + n_m}{n_m}}, \qquad (1)$$

where n_m is the moles of metallic cobalt in these particles, d_1 is the diameter of seed particles formed after the first step of reaction, and d_2 is the diameter of the particles after the second reaction step for which n_i moles of ionic cobalt were added. Since half of the colloid was removed and replaced with an equal amount of ionic cobalt in our experiment, $n_i = n_m$. Then after j steps, the diameter of the particles is given by

$$d_j = 2^{(j-1)/3} d_1 . \qquad (2)$$

Figure 2 compares the particle size calculated from Eq. (2) with the mean particle size directly measured from the TEM negatives. The good agreement between the experimental values and the theory shows that the assumptions implicit in Eq. (2), viz. that no new particles are formed and all the Co^{2+} added after the first step of the reaction is reduced to metal onto the cobalt particles already present, are valid. Moreover, it shows that the desired particle size can be synthesized by controlling the amount of reaction material added into the colloid in each step. However, TEM also showed this procedure cannot be repeated without limit. After four steps of the reaction, a bimodal distribution of particles became evident, which indicates that the surfactant layer on the particle surface has a certain stretching limit. Beyond a certain micelle size, forming new seed particles will be energetically more favorable than increasing the size of the existing particles.

B. Magnetic properties

Because of their small size, anisotropy energy barriers for magnetic nanoparticles are smaller than for the bulk material. Therefore, at high temperature, thermal energy can overcome the anisotropy barrier and allow a coherent rotation of the atomic moments of a particle. Each particle then behaves like a giant atom with a large moment, a phenomenon called superparamagnetism.[11] Only when the temperature drops below the blocking temperature (T_B) will the particle's moment be frozen to its lattice. This creates a peak at the blocking temperature for the zero field cooled (ZFC) magnetization under a small applied field with increasing temperature.

The position of the peak is predicted by Neel's theory[12]

$$25 k_B T_B = K_{\text{eff}} V , \qquad (3)$$

where k_B and K_{eff} are the Boltzmann constant and effective magnetic anisotropy constant, respectively, and V is the average volume of the particles. Most of the early work in this area considered only anisotropy which comes from isolated single particles. However, as El-Hilo *et al.*[13] and Dormann *et al.*[14] pointed out, if the concentration of nanoparticle becomes high enough,

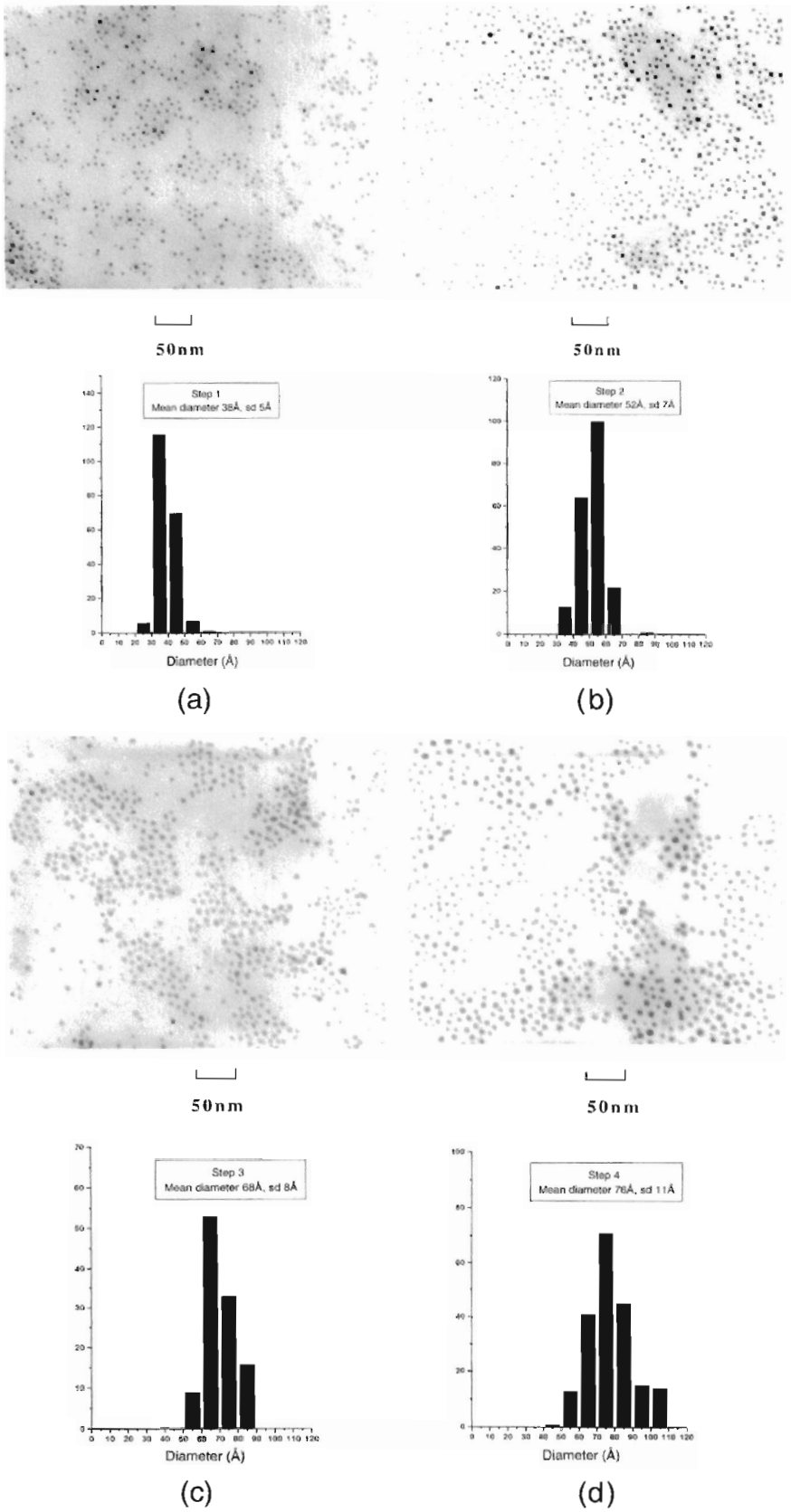

FIG. 1. TEM images and histograms of particles synthesized by the germ-growth method at 10 °C. (a) Step 1, diameter 38 Å; (b) Step 2, diameter 52 Å; (c) Repeat Step 2, diameter 68 Å; (d) Repeat step 2, diameter 76 Å.

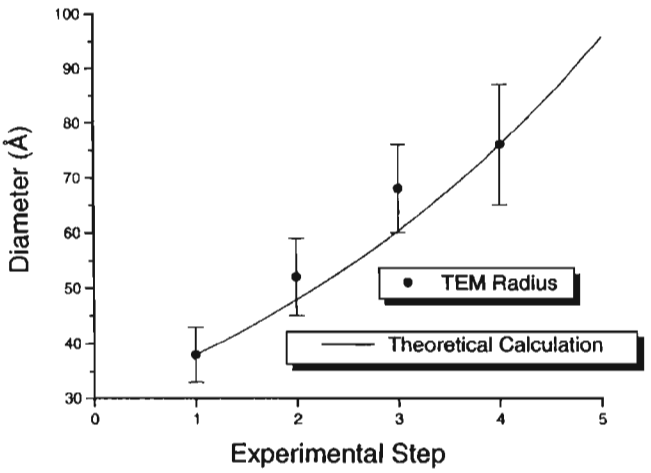

FIG. 2. Comparison between theoretical calculation from Eq. (2) and experimental measurement of particle size.

interparticle interaction will increase the anistropy energy barrier and cause a distinct shift of the blocking temperature. Therefore, effective anisotropy has two contributions.

$$K_{\text{eff}} = K_{intri} + K_{inter}\,, \tag{4}$$

where K_{intri} is the intrinsic anisotropy related to a single particle and K_{inter} is interaction anisotropy as a result of interparticle interaction.

Figure 3 shows the ZFC magnetization versus temperature curves for particles with different sizes. The blocking temperature increased from 29 to 76 K as the particle size increased from 38 to 76 Å. Using the measured T_B and the TEM determined particle volume, we can calculate the effective anisotropy constant from

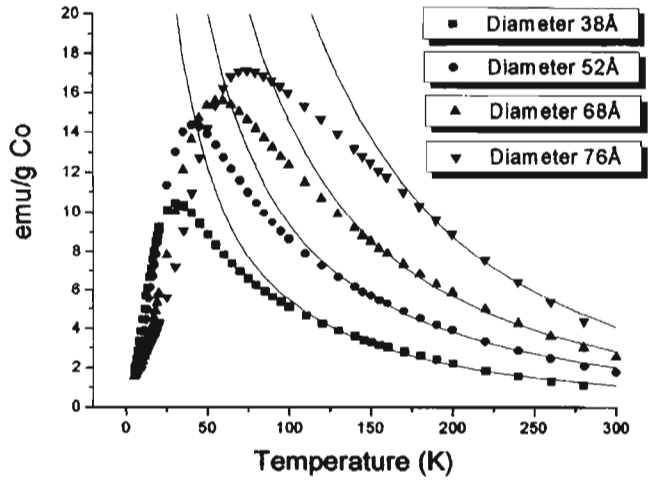

FIG. 3. ZFC magnetization versus temperature for different size particles. Applied magnetic field is 200Oe. Solid lines are fitting curves using Langevin equation with a temperature dependent magnetic moment $\mu_p = \mu_{p0}e^{-cT}$.

Eq. (3). The results are listed in Table I. The anisotropy constant increases as particle size becomes smaller, indicating that the intrinsic surface anisotropy becomes a major effect for smaller particles. At 500 °C, the anisotropy constant of bulk fcc cobalt is 2.3×10^5 erg/cm^3,[15] smaller than the anisotropy constant of the nanoparticles, which are also fcc, at cryogenic temperature. However, a direct comparison is not possible because bulk fcc cobalt exists only at temperature above 400 °C.[15] In addition, the anisotropy constant of hcp bulk cobalt at cryogenic temperature is around 6.8×10^6 erg/cm^3,[16] larger than that of the nanoparticles.

In order to determine whether the effective anisotropy is merely an intrinsic property of the particles, or it has both intrinsic and interaction contributions, we performed a simple dilution experiment. Both the 38 Å sample and 76 Å sample were diluted four times using a solution with the same concentration of surfactant but no cobalt. Figure 4 compares the ZFC curves under 200Oe applied field before and after the dilution. The absolute magnetization value for the diluted sample is not as reliable because the cobalt concentration is very small and a small error in the mass determination could introduce a large error in emu/g. However, we can see that for small size particles, dilution did not affect the position of blocking temperature while dilution decreased the blocking temperature of the large size particle by almost 7 K. The change of blocking temperature in the large particles system indicates that dipolar interaction between these particles is very strong while in small size particle sample dipolar interaction is negligible. The dilution process reduced the interaction between the large size particles and therefore reduce the overall energy barrier. This result is consistent with a simple calculation which shows that in our undiluted systems the interparticle dipolar interaction energy increases eight times as the particle size doubles.

Above the blocking temperature, the magnetization decreases with increasing temperature according to the Langevin equation:

$$M = M_s\left(\coth\ \alpha - \frac{1}{\alpha}\right), \tag{5}$$

where M_s is the saturation magnetization, $\alpha = \mu_p H/k_B T$, μ_p is the average magnetic moment per particle, and H is the applied magnetic field. However, an attempt to fit the equation to the superparamagnetic region of Fig. 3 with a constant magnetic moment was unsuccessful. The experimental magnetization data decreased with temperature faster than the Langevin equation could predict. This is related to the fact that the magnetic moment of the nanoparticles decreases much faster than the corresponding bulk material due to the temperature-induced intraparticle spin disorder. This enhanced temperature dependence has also been reported

TABLE I. Size-dependent magnetic properties of cobalt nanoparticles.

Designated samples	TEM diameter (Å)	T_B (K)	K_{eff} (10^6 erg/cm^3)	μ_{p0} (μ_B)	H_c (Oe)
Co-071A	38	29	3.5	1700	···
Co-071B	52	40	1.9	2900	···
Co-071C	68	58	1.2	5400	···
Co-071D	76	76	1.1	11000	···
Co-073A	44	34	2.6	···	2400
Co-073B	56	49	1.8	···	1500
Co-073C	64	63	1.5	···	1200
Co-073D	88	81	0.8	···	1000

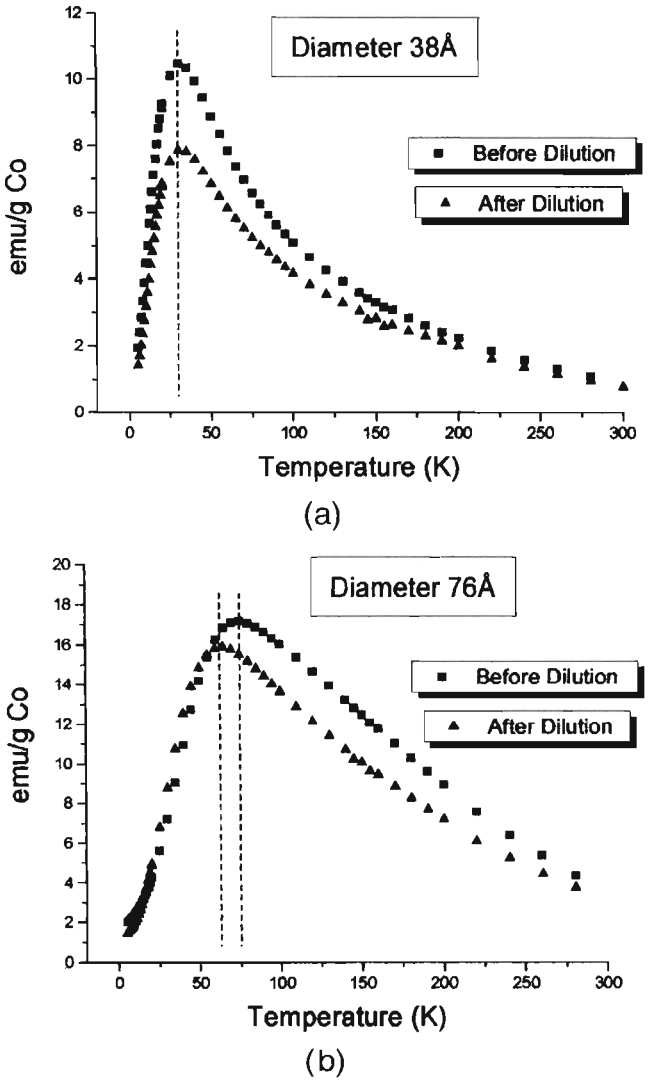

FIG. 4. ZFC magnetization versus temperature curves for (a) 38 Å diameter and (b) 76 Å diameter particles before and after 1 : 4 dilution. Dotted lines are aids for comparison.

in the gas phase experiment[17] and by Monte Carlo calculation.[18] To account for this effect, we introduced an empirical temperature dependent magnetic moment into the Langevin equation, namely $\mu_p = \mu_{p0}e^{-cT}$ (c ranges from 0.010 to 0.020). The solid curves in Fig. 3 are fitting curves of the Langevin equations with a magnetic moment decreasing exponentially as indicated above. The zero temperature magnetic moments μ_{p0} derived from the fitting curves increased from $1700\mu_B$ to $11{,}000\mu_B$ as the particle size increased (Table I) consistent with the change of particle volume.

Theoretical calculations for same size uniaxial particles with easy axis aligned with the applied field showed that coercivity (H_{ci}) is related to the temperature by[19]

$$H_{ci} = \frac{2K_{\text{eff}}}{M_s}\left[1 - \left(\frac{T}{T_B}\right)^{1/2}\right]. \qquad (6)$$

Figure 5 plots the experimental coercivity versus $(T/T_B)^{1/2}$ for different size particles. All sizes have enhanced coercivity compared with the bulk value. Smaller size particles have a higher coercivity than larger size particles consistent with K_{eff} being larger for smaller particles. At very low temperature, all sizes show a small variation of coercivity with temperature, indicating that the thermal energy has a relatively small contribution in the process of reversing the magnetic moment at low temperature. Above the blocking temperature, the particles are superparamagnetic and the coercivities are equal to zero. In the intermediate temperature range, the coercivity decreases with temperature as predicted by Eq. (6) with a strong size-dependent slope. The interception points of linear fitting lines on the $(T/T_B)^{1/2}$ axis range from 0.77 to 0.84, instead of 1 predicted by Eq. (6). This nonunity intercept is largely due to the finite width of the particle size distribution. As an example of the effect of polydispersity, we assume that particle radius has a log-normal distribution

$$f(r) = \frac{1}{\sqrt{2\pi}\ \ln\ \sigma} e^{-\frac{(\ln\frac{r}{r_0})^2}{2(\ln\sigma)^2}}. \qquad (7)$$

We also assume that only T_B in Eq. (6) has a size dependence [through Eq. (3)]. Then the convolution of Eq. (6) with the size distribution of Eq. (7) yields the average coercivity:

$$\langle H_{ci}\rangle = \frac{2K_{\text{eff}}}{M_s}\left[1 - e^{\frac{27}{8}(\ln\sigma)^2}\left(\frac{T}{\langle T_B\rangle}\right)^{1/2}\right]. \qquad (8)$$

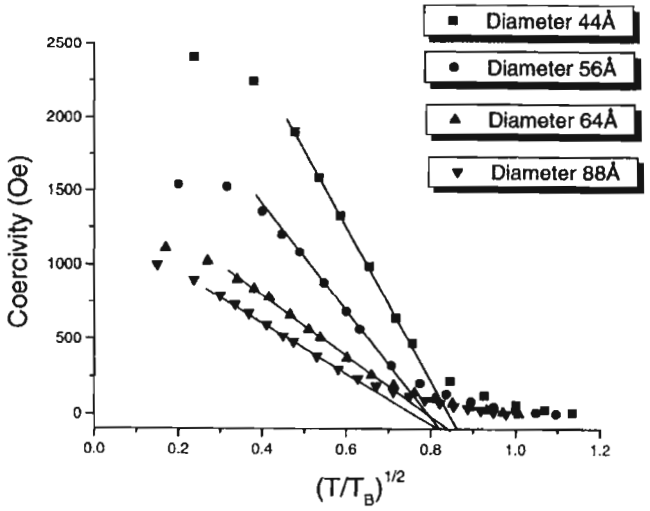

FIG. 5. Magnetic coercivity versus $(T/T_B)^{1/2}$ for different size particles. Solid lines are fitting lines in the intermediate temperature range.

This result shows that when the system is polydisperse, i.e., when $\sigma > 1$, plotting H_c versus $(T/T_B)^{1/2}$ will not have unity intercept as we have observed. In fact, the intercepts of Fig. 4 applied to Eq. (8) yield σ in the range of 1.25 to 1.32 in qualitative agreement with those measured from TEM micrograph (1.1 to 1.2); however, a direct comparison cannot be made because of the incorrect assumption that K_{eff} and M_s are not size-dependent. Regardless, we conclude that the nonunity intercepts in Fig. 4 are due to particle size polydispersity.

The saturation magnetization was also studied for different size particles. Preliminary results show that it is very sensitive to the interaction between the particle surface and coating surfactant, other ligands added in the system, and the post-preparation treatment. Those results will be discussed in our future publications.

IV. CONCLUSION

In summary, we have used the germ-growth method to synthesize different size cobalt particles in inverse micelles. Particle diameter ranged from 38 to 88 Å. This method was proven to be very effective for the control of particle size within a certain size range. Furthermore, the germ-growth method might provide an alternative method to synthesize core-shell type of nanocomposites. The magnetic properties of the cobalt particles produced by this method were studied as a function of size. Both blocking temperatures and coercivity changed with the particle size, as expected from the theory of superparamagnetism. Interparticle interactions were found to be important for larger size particles.

ACKNOWLEDGMENTS

We appreciate the useful discussion with D. Zhang and the help from A. Paulsen with our TEM experiment.

REFERENCES

1. A.P. Alivisatos, Science **271**, 933 (1996); J. Shi, S. Gider, D. Babcock, and D.D. Awschalom, Science **271**, 937 (1996).
2. W.P. Halperin, Rev. Mod. Phys. **58**, 533 (1986).
3. O.I. Micic, H.M. Cheong, H. Fu, A. Zunger, J.R. Sprague, A. Mascarenhas, and A.J. Nozik, J. Phys. Chem. B **101**, 4904 (1997).
4. I.M.L. Billas, A. Chatelain, and W.A. de Heer, Science **265**, 1682 (1994); I.M.L. Billas, A. Chatelain, and W.A. de Heer, J. Magn. Magn. Mater. **168**, 64 (1997); D.C. Douglass, A.J. Cox, J.P. Bucher, and L.A. Bloomfield, Phys. Rev. B **47**, 12874 (1993).
5. M.D. Morse, M.E. Geusic, J.R. Heath, and R.E. Smalley, J. Chem. Phys. **83**, 2293 (1985).
6. J.P. Wilcoxon, R.L. Williamson, and R. Baughman, J. Chem. Phys. **98**, 9933 (1993).
7. L. Motte, F. Billoudet, and M.P. Pileni, J. Phys. Chem. **99**, 16425 (1995); J. Tanori and M.P. Pileni, Langmuir **13**, 639 (1997).
8. X.M. Lin, C.M. Sorensen, K.J. Klabunde, and G.C. Hajipanayis, Langmuir **14**, 7140 (1998).
9. G.N. Glavee, K.J. Klabunde, C.M. Sorensen, and G.C. Hajipanayis, Langmuir **9**, 162 (1993); G.N. Glavee, K.J. Klabunde, C.M. Sorensen, and G.C. Hajipanayis, Inorg. Chem. **32**, 474 (1993).
10. G. Schmid, Chem. Rev. **92**, 1709 (1992).
11. B.D. Cullity, *Introduction to Magnetic Materials* (Addison-Wesley, London, 1972), p. 414.
12. L.C. Neel, Roy. Acad. Sci. **228**, 664 (1949).
13. M. El-Hilo, K. O'Grady, and R.W. Chantrell, J. Magn. Magn. Mater. **114**, 295 (1992).
14. J.L. Dormann, L. Bessasis, and D. Fiorani, J. Phys. C. **21**, 2015 (1988).
15. W. Sucksmith, F.R.S. Thompson, and J.E. Thompson, Proc. Roy. Soc. London **225**, 362 (1954).
16. B.D. Cullity, *Introduction to Magnetic Materials* (Addison-Wesley, London, 1972), p. 236.
17. I.M.L. Billas, A.J. Becker, A. Chatelain, and W.A. de Heer, Phys. Rev. Lett. **71**, 4067 (1993).
18. J.P. Bucher and L.A. Bloomfield, Phys. Rev. B **45**, 2537 (1992).
19. B.D. Cullity, *Introduction to Magnetic Materials* (Addison-Wesley, London, 1972), p. 415.